1 Introduction

Structural problems under mechanical and thermal cyclic loads are frequently encountered in the design problems and are widely used in industry. Since in the advanced design codes such as power piping and pressure vessels, the structure is designed for cyclic loading in the plastic region, the problems related to cyclic response of the structures in the plastic region is of interest for many researchers. The question remains of the true behavior of a structure in regard to the reverse plasticity (or shakedown) or ratcheting. Based on the reverse plasticity, although some inelastic strain accumulates during a few cycles, the rate of accumulated strain tends to become zero by increasing the cycles. On the other hands, it is possible to have a situation where the accumulated inelastic deformation exceeds the allowable value causing structural failure. This behavior is defined as ratcheting.

Many criteria and constitutive models are proposed in the literature to estimate the behavior of a structure under cyclic loading condition. The main differences among these models are related to the hardening theories. Hill (1950) and Westergaard (1952) presented the basic works related to isotropic hardening theory. Based on this theory, the radius of yield surface is extended in the Haigh–Westergaard stress space. Inelastic analysis of a circular rod based on the isotropic hardening model using the von Mises yield criterion is discussed by Neal and Shirvastava (1990). Since isotropic hardening theory does not consider the Bauschinger effect, the response based on this theory does not coincide with the experimental data.

According to the Bauschinger effect, yield surface is transferred in the Haigh–Westergaard stress space during plastic loading. In 1956, the first kinematic rule with linear hardening capable to consider translation of yield surface was proposed by Parger (1958). Ziegler (1959) proposed a kinematic hardening model. This kinematic model is merely able to describe linear hardening, although it is widely used in commercial finite elements codes (Karlsson et al. 2001). Nevertheless, numerous modifications have been propped in order to precisely evaluate the plastic responses, since neither cyclic stress–strain curves nor the hysteresis loop curves can be precisely simulated. Besseling (1959) and Mroz (1967) suggested multi-layer and multi-surface models to overcome the aforementioned defect in the linear kinematic hardening models. However, these models failed to predict the ratcheting phenomenon. Thus, Armstrong and Frederick (1966) proposed a nonlinear kinematic hardening model in 1966. The nonlinear term in this model makes the slope of strain–stress curve different in loading and unloading process and as a result cyclic ratcheting phenomenon is predict more realistically. In 1979, a kinematic hardening model for cyclic plasticity was proposed by Dang-Ban et al. (1979), where the total back stress tensor is decomposed into additive parts with each part following the Armstrong–Frederick hardening model to use the experimental data. In 2006, plastic cyclic behavior of thick pressure vessels using kinematic hardening criterion was studied by Mahbadi and Eslami (2006). The aim of this paper was to compare the Prager linear kinematic hardening with the Armstrong–Frederick nonlinear kinematic hardening model. It was concluded that the linear kinematic hardening of Prager model predicts reverse plasticity for a vessel subjected to all categories of cyclic loadings. On the other hands, the nonlinear theory of Armstrong–Frederick results in ratcheting responses for the load-controlled cyclic loadings, reverse plasticity for the strain controlled cyclic loadings with zero mean load, and thermal cyclic loadings with zero and non-zero mean load. Also, Mahbadi et al. (2013, 2017) have investigated cyclic behavior of thick spherical and cylindrical vessels, respectively, made of transversely isotropic materials using anisotropic yield criterion. As a result, identical behaviors similar to Mahbadi and Eslami (2006) study are observed for these materials.

Rusinko and Rusinko (2009, 2011) described the synthetic flow theory, where a corner point along the loading path on the yield surface is produced, and considerably widened the

applicability of this theory. Regarding the importance of cyclic loading, recent studies are conducted into this field. The book written by Shorr in 2005 is among these works (Shorr 2015). In this book, recent investigations on integrity of materials at high temperature are presented. Moreover, developed numerical methods for thermo-cyclic creep are presented. Since analysis of plastic deformation is required for mechanical design of the structures subjected to cyclic loading, Hashiguchi (2017) assessed and reviewed the cyclic plasticity models in 2017. In 2017, cyclic deformation of Inconel 718 superalloy was modeled by means of crystal plasticity by Cruzado et al. (2017). The computational homogenization and a linear jump approach was developed to diminish the computational time for simulating numerous cycles. Roostaei and Jahed (2018) developed a cyclic small-strain plasticity model for anisotropic wrought Mg alloy under multiaxial loading.

Chaboche (1986) proposed a time-independent constitutive model for cyclic plasticity, which combines the nonlinear kinematic hardening and isotropic hardening theories. The model is capable to estimate the cyclic loading behavior of a structure more accurately compared to the previous linear kinematic hardening models. Cyclic plastic responses of beams based on the time-independent Chaboche hardening model is investigated by Shojaei et al. (2010). It is concluded that this model predicts reverse plasticity for deformation (strain) controlled conditions and load-controlled stresses with zero mean stress. A ratcheting response is observed for the load-controlled conditions with non-zero mean stress.

In the past decades, a several viscoplasticity constitutive models are proposed to predict the structural behavior under cyclic loading condition at high elevated temperatures. Chaboche and Rousselier (1983a,b) proposed the unified viscoplastic constitutive model. In this model, the kinematic and isotropic hardening theories are considered in a unified form. Contrary to 1986 Chaboche model (Chaboche 1986), this theory is a time-dependent model which is able to evaluate effects of rate and creep time and also it is suitable for high temperature conditions, where rate effect is important. This model is widely accepted in the literature. The key problem to properly use this model is how to select the initial set of the material properties which are used in the model. This problem is resolved and referred in the literature by a number of authors such as Zhan et al. (2004), Zhan (2004), and Gong et al. (2010).

Since improving the knowledge of the rate-dependent behavior of materials is of significant importance in many engineering applications, many cyclic loading researches deal with modifying rate-dependent constitutive models. Zhu et al. (2016) proposed a thermo-mechanically coupled cyclic elasto-viscoplastic constitutive model of metals and implemented it into a finite element code (ABAQUS). The proposed model is verified by comparing with the experimental results of 316L stainless steel. In 2017 a modified constitutive model is proposed based on the unified viscoplasticity theory considering time-dependent kinematic hardening for relaxation by Chen et al. (2017). Hang et al. (2019) used a modified unified viscoplastic constitutive model to evaluate the axial torsional thermo-mechanical cyclic loading. In 2018, a series of experiments were conducted by Chen et al. (2018) to determine the creep and fatigue behavior of 316 stainless steel and to revisit a unified viscoplastic model. Benaarbia et al. (2018) have developed a thermodynamically-based viscoelastic–viscoplastic model for the high temperature cyclic behavior of 9–12% Cr steels, considering the isotropic and kinematic hardening theories. Rae et al. (2019) studied experimental characterisation and computational modeling of cyclic viscoplastic behavior of turbine steel. In addition, changes in stress ranges hysteresis area and viscous stress were analyzed in order to characterize the cyclic mechanical behavior of the FV566 steel. The rate-dependent ratcheting characteristics of 35CRMo alloy have been investigated by Zheng et al. (2019) under cyclic uniaxial tension considering different stress amplitudes at high temperature.

There are also other papers deal with viscoplastic constitutive models such as those studied by Dong et al. (2014), Chen and Feng (2015), Szmytka et al. (2015), Kyaw et al. (2016), Ahmed et al. (2016), Luk-Cyr et al. (2017) and Xiaoan et al. (2019).

In this study the Chaboche unified viscoplastic model (Chaboche and Rousselier 1983a,b), which is a time-dependent model with combined kinematic and isotropic hardening theories, is considered. The model allows one to reasonably predict the behavior of materials under cyclic loading condition. It must be mentioned that some limitations exist on application of isotropic hardening theory as described in synthetic flow theory by Rusinko and Rusinko (2009, 2011). The assumed vessel material is considered to be type 316 stainless steel, where to obtain the coefficients and parameters of the material for starting point of cyclic loading (Gong et al. 2010). The numerical analysis is carried out using the experimental results of type 316 stainless steel. Due to nonlinearity of the problem and applying the combined isotropic and kinematic hardening theories of plasticity, a numerical method is proposed to solve the governing partial differential equations of the problem. The plastic and creep strains are obtained by a unified flow rule. The proposed numerical method is the modification of the method proposed by Mahbadi and Eslami (2006), Mahbadi et al. (2013, 2017), Shojaei et al. (2010), where the generalized differential quadrature (GDQ by Shu 2012) method is used to calculate the stress tensor. The novelty of the present study, in comparison with the published papers reported on cyclic loading, is application of a time-dependent constitutive model to obtain both plastic and creep strains due to the combination of thermal and mechanical loads. Temperature-dependent material properties is considered and the GDQ method is employed to solve the governing differential equations. The cyclic viscoplastic behavior of thick spherical pressure vessels is derived and presented. The basic concern of this paper is to show that cyclic loading of strain controlled loads results in shakedown or reversed plasticity.

2 Mathematical formulation

A thick spherical vessel made of isotropic material is considered. The vessel is subjected to the combination of thermal and mechanical loads. The inside and outside radius of vessel, R_1 and R_2, are subjected to inside and outside pressures P_1 and P_2 and inside and outside temperatures T_1 and T_2, respectively. The following normalized parameters are considered in Eq. (1) to conveniently obtain convergence:

$$
\begin{aligned}
&\bar{\sigma}_{rr} = \frac{\sigma_{rr}}{\sigma_0}, \quad \bar{\sigma}_{\theta\theta} = \frac{\sigma_{\theta\theta}}{\sigma_0}, \quad \bar{\sigma}_{\phi\phi} = \frac{\sigma_{\phi\phi}}{\sigma_0}, \quad \bar{\epsilon}_{rr} = \frac{\epsilon_{rr}}{\epsilon_0},\\
&\bar{\epsilon}_{\theta\theta} = \frac{\epsilon_{\theta\theta}}{\epsilon_0}, \quad \bar{\epsilon}_{\phi\phi} = \frac{\epsilon_{\phi\phi}}{\epsilon_0}, \quad \bar{\epsilon}^{in}_{rr} = \frac{\epsilon^{in}_{rr}}{\epsilon_0}, \quad \bar{\epsilon}^{in}_{\theta\theta} = \frac{\epsilon^{in}_{\theta\theta}}{\epsilon_0},\\
&\bar{\epsilon}^{in}_{\phi\phi} = \frac{\epsilon^{in}_{\phi\phi}}{\epsilon_0}, \quad \bar{\epsilon}^{\mathrm{Res}}_{rr} = \frac{\epsilon^{\mathrm{Res}}_{rr}}{\epsilon_0}, \quad \bar{\epsilon}^{\mathrm{Res}}_{\theta\theta} = \frac{\epsilon^{\mathrm{Res}}_{\theta\theta}}{\epsilon_0}, \quad \bar{\epsilon}^{\mathrm{Res}}_{\phi\phi} = \frac{\epsilon^{\mathrm{Res}}_{\phi\phi}}{\epsilon_0},\\
&\bar{P}_1 = \frac{P_1}{\sigma_0}, \quad \bar{P}_2 = \frac{P_2}{\sigma_0}, \quad \rho = \frac{r}{R_1}, \quad \beta = \frac{R_2}{R_1}, \quad \tau = \frac{E_0\alpha_0 T}{\sigma_0(1-\nu)}.
\end{aligned}
\tag{1}
$$

In Eqs. (1) σ_{ij} is the stress tensor and ϵ_{ij} is the strain tensor. The subscripts rr, $\theta\theta$, and $\phi\phi$ describe the radial, tangential, and meridional directions, respectively. Also, ϵ^{in} and ϵ^{Res} represent the inelastic strain and residual strain, respectively. The parameters σ_0 and ϵ_0 are

the initial yield stress and the initial yield strain, and T is the temperature distribution in the vessel. The dimensionless stress–strain relations in spherical coordinate are as follows:

$$\begin{aligned}
\bar{\epsilon}_{rr} &= \frac{1}{\bar{E}}\left[\bar{\sigma}_{rr} - \nu(\bar{\sigma}_{\theta\theta} + \bar{\sigma}_{\phi\phi})\right] + \bar{\alpha}(1-\nu)\tau + \bar{\epsilon}_{rr}^{in} + \bar{\epsilon}_{rr}^{\mathrm{Res}},\\
\bar{\epsilon}_{\theta\theta} &= \frac{1}{\bar{E}}\left[\bar{\sigma}_{\theta\theta} - \nu(\bar{\sigma}_{rr} + \bar{\sigma}_{\phi\phi})\right] + \bar{\alpha}(1-\nu)\tau + \bar{\epsilon}_{\theta\theta}^{in} + \bar{\epsilon}_{\theta\theta}^{\mathrm{Res}},\\
\bar{\epsilon}_{\phi\phi} &= \frac{1}{\bar{E}}\left[\bar{\sigma}_{\phi\phi} - \nu(\bar{\sigma}_{rr} + \bar{\sigma}_{\theta\theta})\right] + \bar{\alpha}(1-\nu)\tau + \bar{\epsilon}_{\phi\phi}^{in} + \bar{\epsilon}_{\phi\phi}^{\mathrm{Res}},
\end{aligned} \tag{2}$$

where

$$\begin{aligned}
\bar{E} &= \frac{E}{E_0},\\
\bar{\alpha} &= \frac{\alpha}{\alpha_0}.
\end{aligned} \tag{3}$$

In Eqs. (2), ν is Poisson's ratio and α_0 is the initial thermal expansion. Due to the spherical symmetry, $\bar{\sigma}_{\theta\theta} = \bar{\sigma}_{\phi\phi}$ and $\bar{\epsilon}_{\theta\theta} = \bar{\epsilon}_{\phi\phi}$. By substituting Eqs. (2) into the one-dimensional compatibility equation and using the equilibrium equation in a spherical coordinates system, a second order non-homogeneous differential equation with variable coefficients for $\bar{\sigma}_{rr}$ is obtained, as given by the following equation (Hetnarski and Eslami 2019):

$$\left(\frac{B\rho}{2}\right)\frac{d^2\bar{\sigma}_{rr}}{d\rho^2} + \left(2B - \frac{\rho BA}{2}\right)\frac{d\bar{\sigma}_{rr}}{d\rho} + \left(AC'\right)\bar{\sigma}_{rr} = D + F' + G \tag{4}$$

where

$$\begin{aligned}
A &= \frac{1}{\bar{E}}\frac{d\bar{E}}{d\rho}, \qquad B = \frac{(1-\nu)}{\bar{E}}, \qquad C' = \frac{1}{\bar{E}},\\
D &= \frac{3}{2\rho}\bar{\epsilon}_{rr}^{in} + \frac{3}{2\rho}\bar{\epsilon}_{rr}^{\mathrm{Res}},\\
F' &= -(1-\nu)\left(\frac{d\bar{\alpha}}{d\rho}\tau + \frac{d\tau}{d\rho}\bar{\alpha}\right),\\
G &= \frac{1}{2}\frac{d\bar{\epsilon}_{rr}^{in}}{d\rho} + \frac{1}{2}\frac{d\bar{\epsilon}_{rr}^{\mathrm{Res}}}{d\rho}.
\end{aligned} \tag{5}$$

The heat conduction equation in the steady-state condition for the one-dimensional problem in spherical coordinates is given by

$$\frac{d}{dr}\left(k'r^2\frac{dT}{dr}\right) = 0 \tag{6}$$

where k' is the thermal conduction coefficient being assumed to be temperature dependent. We may assume the following form for k':

$$k' = \xi_1 T + \xi_2. \tag{7}$$

The dimensionless temperature distribution is obtained by integrating Eq. (6) twice,

$$\tau = \frac{\xi_2}{\xi_1} + \left[\left(\frac{\xi_2}{\xi_1}\right)^2 - \frac{2}{\xi_1}\left(\frac{\Gamma_1}{\rho} - \Gamma_2\right)\right]^{\frac{1}{2}}. \tag{8}$$

Using the boundary conditions $T(R_1) = T_1$ and $T(R_2) = T_2$ to determine the constants Γ_1 and Γ_2, yields

$$\begin{aligned} \Gamma_1 &= \frac{\beta}{\beta - 1}\left[\frac{\xi_1}{2}\left(\tau_2^2 - \tau_1^2\right) - \xi_2(\tau_2 - \tau_1)\right], \\ \Gamma_2 &= \frac{1}{\beta - 1}\left[\frac{\xi_1}{2}\left(\beta\tau_2^2 - \tau_1^2\right) - \xi_2(\beta\tau_2 - \tau_1)\right]. \end{aligned} \tag{9}$$

In exploring an effective discretization method, Bellman and Casti (1971), Kashef et al. (1972) proposed the differential quadrature method (DQM). The weight coefficient in the DQ must be determined for the discretization of a derivative of any order. Two approaches are proposed in Bellman and Casti (1971) to define the weighting coefficients of the first order derivative. First, by accomplishing an algebraic equation system and second by considering a simple algebraic formulation. Since the number of grid points in Bellman's approach was limited, Shu (2012) introduced a method to calculate the weight coefficient for the first and higher order derivatives with arbitrary number and distribution of grid points, which then was defined as the GDQ method. Using the GDQ method, the rth order derivative of function $f(x_i)$ is defined as

$$\left.\frac{d^r f(x)}{dx^r}\right|_{x=x_i} = \sum_{j=1}^{N} c_{ij}^{(r)} f(x_j). \tag{10}$$

Thus, the first and second order derivatives of radial stress $\frac{d\bar{\sigma}_{rr}}{d\rho}$ and $\frac{d^2\bar{\sigma}_{rr}}{d\rho^2}$ are defined as

$$\begin{aligned} \left.\frac{d\bar{\sigma}_{rr}}{d\rho}\right|_{\rho=\rho_i} &= \sum_{j=1}^{N} c_{ij}^{(1)} \bar{\sigma}_{rr}(\rho_j), \\ \left.\frac{d^2\bar{\sigma}_{rr}}{d\rho^2}\right|_{\rho=\rho_i} &= \sum_{j=1}^{N} c_{ij}^{(2)} \bar{\sigma}_{rr}(\rho_j), \end{aligned} \tag{11}$$

where N is the number of grid points along the radial direction and $c_{ij}^{(1)}$ can be obtained by the following relations:

$$\begin{aligned} c_{ij}^{(1)} &= \frac{M^{(1)}(\rho_i)}{(\rho_i - \rho_j)M^{(1)}(\rho_j)}, \quad i \neq j,\ i, j = 1, 2, \ldots, N, \\ c_{ii}^{(1)} &= -\sum_{j=1, j\neq i}^{N} c_{ij}^{(1)}, \quad i = 1, 2, \ldots, N, \end{aligned} \tag{12}$$

where $M(\rho)$ is defined as

$$M(\rho) = \prod_{j=1}^{N}(\rho - \rho_j) \tag{13}$$

and also $M^{(1)}(\rho)$ can be obtained:

$$M^{(1)}(\rho_i) = \prod_{j=1, j\neq i}^{N} (\rho_i - \rho_j). \tag{14}$$

Using $c_{ij}^{(1)}$, the weighting coefficient $c_{ij}^{(2)}$ along the radial direction can be defined as

$$\begin{aligned} c_{ij}^{(2)} &= 2\left(c_{ii}^{(1)} c_{ij}^{(1)} - \frac{c_{ij}^{(1)}}{\rho_i - \rho_j}\right), \quad i \neq j,\ i, j = 1, 2, \ldots, N, \\ c_{ii}^{(2)} &= -\sum_{j=1, j\neq i}^{N} c_{ij}^{(2)}, \quad i = 1, 2, \ldots, N. \end{aligned} \tag{15}$$

In order to obtain a better distribution for mesh points along the radial direction, the Chebyshev–Gauss–Lobatto technique is applied as

$$\rho_i = \frac{(\beta - 1)}{2}\left[1 - \cos\left(\frac{i-1}{N-1}\pi\right)\right] + 1. \tag{16}$$

Using the GDQ method and substituting Eqs. (11) into Eq. (4), the radial stress in the grid points can be obtained:

$$\left[K^{(1)}\right]\{\bar{\sigma}_{rr}\} = \{F\} \tag{17}$$

where the components of stiffness matrix $[K^{(1)}]$ can be obtained by the following equations:

$$\begin{aligned} k_{ij}^{(1)} &= \left(\frac{B_i \rho_i}{2}\right) c_{ij}^{(2)} + \left(2B_i - \frac{\rho B_i A_i}{2}\right) c_{ij}^{(1)}, \quad i \neq j, \\ k_{ij}^{(1)} &= \left(\frac{B_i \rho_i}{2}\right) c_{ij}^{(2)} + \left(2B_i - \frac{\rho B_i A_i}{2}\right) c_{ij}^{(1)} + A_i C_i', \quad i = j. \end{aligned} \tag{18}$$

Using Eqs. (5) and (8), A_i, B_i and C_i' are defined as follows:

$$\begin{aligned} A_i &= \frac{1}{\bar{E}_i}\frac{d\bar{E}}{d\tau}\bigg|_{\rho=\rho_i} \frac{d\tau}{d\rho}\bigg|_{\rho=\rho_i} = \frac{1}{\bar{E}_i}\frac{d\bar{E}}{d\tau}\bigg|_{\rho=\rho_i} \frac{\Gamma_1}{[\xi_1 + \tau(\rho_i) + \xi_2]\rho_i^2}, \\ B_i &= \frac{(1-\nu)}{\bar{E}_i}, \\ C_i' &= \frac{1}{\bar{E}_i}, \end{aligned} \tag{19}$$

where $\bar{E}_i$ is the normalized elasticity modulus at ρ_i radius. The force vector is defined as

$$f_i = D_i + F_i' + G_i. \tag{20}$$

In order to calculate G_i, the GDQ method is applied to $\frac{d\bar{\epsilon}_{rr}^{in}}{d\rho}$ and $\frac{d\bar{\epsilon}_{rr}^{\mathrm{Res}}}{d\rho}$:

$$G_i = \frac{1}{2}\sum_{j=1}^{N} c_{ij}^{(1)} \bar{\epsilon}_{rr}^{in}(\rho_j) + \frac{1}{2}\sum_{j=1}^{N} c_{ij}^{(1)} \bar{\epsilon}_{rr}^{\mathrm{Res}}(\rho_j). \tag{21}$$

Using Eqs. (5) and (8), D_i and F_i' are defined as

$$\begin{aligned} D_i &= \frac{3}{2\rho}\bar{\epsilon}_{rr}^{in}\big|_{\rho=\rho_i} + \frac{3}{2\rho}\bar{\epsilon}_{rr}^{\mathrm{Res}}\big|_{\rho=\rho_i}, \\ F_i' &= -(1-\nu)\frac{d\tau}{d\rho}\bigg|_{\rho=\rho_i}\left(\frac{d\bar{\alpha}}{d\tau}\bigg|_{\rho=\rho_i}\tau(\rho_i) + \bar{\alpha}_i\right), \end{aligned} \tag{22}$$

where $\bar{\alpha}_i$ is the normalized thermal expansion coefficient at ρ_i radius.

After evaluating the radial stresses of grid points, the tangential stresses can be calculated using the equilibrium equation. The GDQ discretization method is applied to this equation and the tangential stresses of the grid points are obtained:

$$\{\bar{\sigma}_{\theta\theta}\} = \left[K^{(2)}\right]\{\bar{\sigma}_{rr}\} \tag{23}$$

where the elements of $[K^{(2)}]$ matrix are defined as

$$\begin{aligned} k_{ij}^{(2)} &= \frac{\rho_i}{2}c_{ij}^{(1)}, \quad i \neq j, \\ k_{ij}^{(2)} &= \frac{\rho_i}{2}c_{ij}^{(1)} + 1, \quad i = j. \end{aligned} \tag{24}$$

To impose the boundary conditions of pressure for the spherical vessel, $\bar{\sigma}_{rr}(1) = -\bar{P}_1$ and $\bar{\sigma}_{rr}(\beta) = -\bar{P}_2$, the following modification should be applied to the stiffness matrix $[K^{(1)}]$:

$$\begin{aligned} k_{1j}^{(1)} &= 0, \quad j = 2, \ldots, N, \; k_{11}^{(1)} = 1, \\ k_{Nj}^{(1)} &= 0, \quad j = 1, \ldots, N-1, \; k_{NN}^{(1)} = 1, \end{aligned} \tag{25}$$

and the force vector $\{F\}$ is altered as

$$\begin{aligned} f_1 &= -\bar{P}_1, \\ f_n &= -\bar{P}_2. \end{aligned} \tag{26}$$

3 Unified viscoplastic constitutive model

The Chaboche unified viscoplastic constitutive model (Chaboche and Rousselier 1983a,b) is used to evaluate the cyclic viscoplasticity of the thick spherical vessels subjected to thermo-mechanical loads. The presented constitutive model can be exploited for monotonic or cyclic loading conditions or for a more complex situation (Lemaitre 2001). This model is based on the rate-dependent flow rule which consists of the kinematic and isotropic hardening theories using the normality rule. In order to obtain the inelastic strain rate, the flow rule for this model is

$$\dot{\epsilon}_{ij}^{in} = \frac{3}{2}\dot{\epsilon}^{in}\frac{\sigma_{ij}' - \chi_{ij}'}{J(\sigma_{ij} - \chi_{ij})} = \frac{3}{2}\left\langle\frac{J(\sigma_{ij} - \chi_{ij}) - R - Y}{Z}\right\rangle^n \frac{\sigma_{ij}' - \chi_{ij}'}{J(\sigma_{ij} - \chi_{ij})}. \tag{27}$$

The yield criterion associated with the above constitutive model is

$$f = J(\sigma_{ij} - \chi_{ij}) - R - Y. \tag{28}$$

The McCauley bracket $\langle . \rangle$ is used here to ensure that when $f < 0$, the state of stress is inside the elastic domain. In Eqs. (27) and (28), χ_{ij} is the back stress tensor, n and Z are material parameters which are functions of the temperature, Y is the yield stress and is a function of the temperature, R is associated parameter of the isotropic hardening of material and is called the drag stress, σ'_{ij} and χ'_{ij} are deviatoric stress and back stress tensors and J represents a distance in the stress space which for the von Mises yield criterion is

$$J(\sigma_{ij} - \chi_{ij}) = \left[\frac{3}{2}\left(\sigma'_{ij} - \chi'_{ij}\right)\left(\sigma'_{ij} - \chi'_{ij}\right)\right]^{1/2}. \tag{29}$$

In the present model, the back stress tensor, which is related to the kinematic hardening theory, is described by Eq. (30),

$$\dot{\chi}_{ij} = \dot{\chi}_{ij}^{(1)} + \dot{\chi}_{ij}^{(2)} \tag{30}$$

where $\dot{\chi}_{ij}^{(1)}$ and $\dot{\chi}_{ij}^{(2)}$ are the nonlinear kinematic hardening parameters:

$$\begin{aligned} \dot{\chi}_{ij}^{(1)} &= C_1\left(a_1\dot{\epsilon}_{ij}^{in} - \chi_{ij}^{(1)}\dot{\epsilon}^{in}\right), \\ \dot{\chi}_{ij}^{(2)} &= C_2\left(a_2\dot{\epsilon}_{ij}^{in} - \chi_{ij}^{(2)}\dot{\epsilon}^{in}\right), \end{aligned} \tag{31}$$

where C_1, C_2, a_1, and a_2 are material parameters for the Chaboche kinematic hardening model and are obtained from the uniaxial test and they are considered to be functions of the temperature. The drag stress related to the increase of the yield surface is defined as

$$\dot{R} = b(Q - R)\dot{\epsilon}^{in} + H\dot{\epsilon}^{in}. \tag{32}$$

In Eq. (32), b and Q are material parameters for the isotropic hardening model and they are considered to be temperature dependent. The second term in Eq. (32), $(H\dot{\epsilon}^{in})$, represents the linear evolution of drag stress and is proportional to the effective inelastic strain.

The dimensionless quantities of hardening model are defined as

$$\begin{aligned} &\bar{f} = \frac{f}{\sigma_0}, \quad \bar{C}_k = \frac{C_k}{E_0}, \quad \bar{a}_k = \frac{a_k}{\sigma_0}, \quad \bar{\chi} = \frac{\chi}{\sigma_0}, \quad \bar{Y} = \frac{Y}{\sigma_0}, \\ &\bar{R} = \frac{R}{\sigma_0}, \quad \bar{Z} = \frac{Z\epsilon_0^{1/n}}{\sigma_0}, \quad \bar{Q} = \frac{Q}{\sigma_0}, \quad \bar{b} = \frac{b\sigma_0}{E_0}, \quad \bar{H} = \frac{H}{E_0}. \end{aligned} \tag{33}$$

4 Numerical solution

In this section, the numerical solution procedure for inelastic analysis and cyclic loading behavior of thick spherical vessels under mechanical and thermal loads is described. Due to the existence of ϵ_{rr}^{in} in the force vector, the relations are nonlinear and the inelastic strains are dependent on the loading path and the stress tensor. A numerical iterative procedure based on the successive approximation method is proposed in the present work to evaluate the inelastic analysis of thick vessels. The numerical method described by Mahbadi and Eslami (2006), Mahbadi et al. (2013, 2017), Shojaei et al. (2010) is modified and developed for the viscoplastic material, considering creep analysis, to solve the problem. Successive coordinate systems, corresponding to each cycle during the loading and unloading, are considered by this method. The solution obtained by this successive coordinate systems is

transferred to the main coordinate system located at the beginning of the first cycle of load. Thus, the coordinate system corresponding to the first cycle of the load is identical with the main coordinate system. When the number of cycles are increased, the subsequent successive coordinate systems differ with the main coordinate system. The problem is solved in each successive coordinate system independently, while the parameters such as back stress and residual stresses are initialized based on the results obtained in the previous coordinate system and transferred to the current coordinate system employing proper coordinate transformation. The details of the modified method for viscoplastic thermo-mechanical load is described by the following steps:

- Step 1: Since the modulus of elasticity and yield stress vary at different temperatures, all the input quantities are normalized with the initial yield stress and elasticity modulus.
- Step 2: Total time is divided into p steps and applied load associated with the time division (Load $= f(t)$) is divided into q steps. Also, the cross section of thick sphere is divided into N layers.
- Step 3: For each layer, the yield criteria from Eq. (28) is checked to determine if the layer is in inelastic zone. For the layers that are in the inelastic range, a value for the inelastic strain increment $\Delta\bar{\epsilon}^{in}$ is assumed and is added to the accumulated inelastic strain from the previous step of loading (i.e. for the first increment of inelastic strain the accumulated inelastic strain is zero) to obtain the total inelastic strain.
- Step 4: To determine material properties of each layer, including yield stress, elastic modulus, isotropic and kinematic hardening parameters, and creep parameters, the temperature distribution from Eq. (8) is used. The quadratic equation, given by Eq. (34), is used to approximate these material properties,

$$\lambda = \zeta_1 T^2 + \zeta_2 T + \zeta_3 \tag{34}$$

  where λ is any material property and ζ_1, ζ_2, and ζ_3 are calculated from the experimental data.
- Step 5: Considering the initial guess for $\Delta\bar{\epsilon}^{in}$ in Step 3 and the yield stress from Step 4, the inelastic strain increment tensor using the flow rule, Eqs. (35), is obtained and added to the accumulated inelastic strain to calculate the total inelastic strain,

$$\begin{aligned} \Delta\bar{\epsilon}_{ij}^{in} &= \frac{3}{2}\Delta\bar{\epsilon}^{in}\frac{\bar{\sigma}'_{ij} - \bar{\chi}'_{ij}}{\bar{J}}, \\ \bar{\epsilon}_{ij}^{in} &= \bar{\epsilon}_{ij}^{in(\mathrm{acc})} + \Delta\bar{\epsilon}_{ij}^{in}. \end{aligned} \tag{35}$$

  It must be mentioned that since $\bar{J}$, $\bar{\chi}$, $\bar{\sigma}$ parameters are dependent on inelastic strains, the values of the previous time step are used in this step.
- Step 6: The increment of back stress tensor related to the kinematic hardening theory is obtained from Eqs. (36)

$$\begin{aligned} \Delta\bar{\chi}_{ij}^{(n)} &= \bar{C}_n\left(\bar{a}_n\Delta\bar{\epsilon}_{ij}^{in} - \bar{\chi}_{ij}^{(n)}\Delta\bar{\epsilon}^{in}\right), \\ \Delta\bar{\chi}_{ij} &= \sum_{n=1}^{2}\Delta\bar{\chi}_{ij}^{(n)}, \\ \bar{\chi}_{ij} &= \bar{\chi}_{ij}^{\mathrm{acc}} + \Delta\bar{\chi}_{ij}. \end{aligned} \tag{36}$$

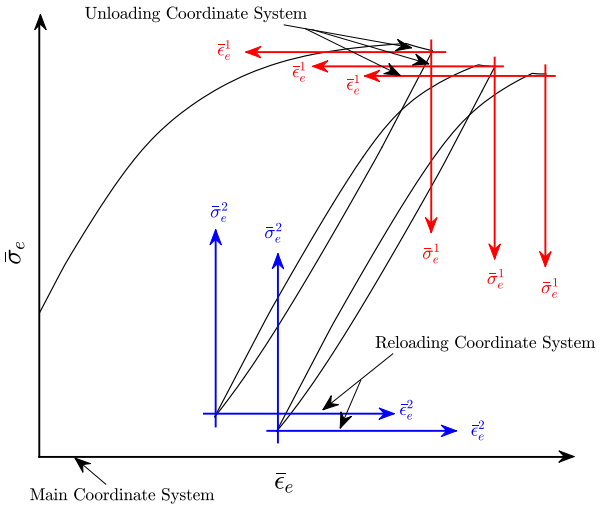

Fig. 1 Unloading and reloading coordinate systems

- Step 7: The extension of radius of the yield surface, using the approximated inelastic strains in Step 5, is obtained:

$$\begin{aligned} \Delta\bar{R} &= \bar{b}(\bar{Q}-\bar{R})\Delta\bar{\epsilon}^{in} + H\Delta\bar{\epsilon}^{in}, \\ \bar{R} &= \bar{R}^{\text{acc}} + \Delta\bar{R}. \end{aligned} \tag{37}$$

- Step 8: The new values of inelastic strains obtained from Step 5 are used to calculate the new values for the radial and tangential stresses by applying new values of inelastic strains to the force vector in the GDQ method, Eq. (20).
- Step 9: Using the calculated quantities in Steps 6 to 8, new inelastic effective strain increment is obtained from Eq. (38),

$$\Delta\bar{\epsilon}^{in} = \left\langle \frac{\bar{J}(\bar{\sigma}_{ij}-\bar{\chi}_{ij}) - \bar{R} - \bar{Y}}{\bar{Z}} \right\rangle^{n} \Delta t. \tag{38}$$

- Step 10: The new values of inelastic strain increments are compared with the initial guess and if the difference between these two values is small enough, repeat the method from Steps 3 to 10. Otherwise, Steps 5 to 10 must be repeated until convergence occurs. The following relative error is considered to determine convergency:

$$\left| \frac{\Delta\bar{\epsilon}_{in}^{\text{New}} - \Delta\bar{\epsilon}_{in}^{\text{Previous}}}{\Delta\bar{\epsilon}_{in}^{\text{New}}} \right| < \text{Tolerance}. \tag{39}$$

- Step 11: For the unloading procedure, a second coordinate system in reverse directions is mounted at the current state of stress and strain values; see Fig. 1.
- Step 12: All the values of stress, strain, accumulated, and total plastic strains are set to zero. The values for back stress and drag stress are transferred to the unloading coordinate system as

$$\bar{\chi}_{ij}^{\text{acc}} = \bar{\sigma}_{ij}^{(2)} - \bar{\chi}_{ij} \tag{40}$$

where $\bar{\chi}_{ij}$ is the accumulated back stress tensor in the unloading coordinate system and $\bar{\sigma}_{ij}^{(2)}$ is the maximum stress tensor in the loading coordinate system.

- Step 13: Steps 2 through 10 are repeated to evaluate the unloading responses. All the calculated quantities in the unloading coordinate systems can be transferred to the main coordinate using the following transmission relation:

$$S_{ij} = \left(\sum_{k=1}^{m} S_{ij}^{L(k)} - \sum_{k=1}^{m-1} S_{ij}^{UL(k)} \right) - S_{ij}^{UL(m)} \tag{41}$$

where S_{ij} is any tensors including stress, total strain, inelastic strain, and back stress. Superscripts $L(k)$ indicate the final value of S_{ij} in kth cycle of loading. Also, $UL(k)$ indicates the final value of S_{ij} in the kth cycle of unloading. Here, m shows the last cycle.

- Step 14: For the reloading procedure, a third coordinate system is attached to the current state of stress and strain values in the same direction of the main coordinate system. All values of stress, strain, accumulated, and total plastic strains are set equal to zero. The values for back stress and drag stress are transferred into the reloading coordinate system as

$$\bar{\chi}_{ij}^{\text{acc}} = \bar{\sigma}_{ij}^{(1)} - \bar{\chi}_{ij} \tag{42}$$

where $\bar{\chi}_{ij}^{\text{acc}}$ is the accumulated back kinematic hardening parameter in the reloading coordinate system and $\bar{\sigma}_{ij}^{(1)}$ is the maximum stress tensor in the unloading coordinate system.

- Step 15: Similar to unloading process, Steps 2 through 10 are repeated in order to estimate the reloading responses. All the calculated quantities in the reloading coordinate systems can be transferred to the main coordinate using the following transmission relation:

$$S_{ij} = \left(\sum_{k=1}^{m-1} S_{ij}^{L(k)} - \sum_{k=1}^{m-1} S_{ij}^{UL(k)} \right) + S_{ij}^{UL(m)}. \tag{43}$$

- Step 16: Procedures between Steps 2 through 15 are repeated until the final cycle of load is archived.

The flow chart corresponding to the proposed numerical procedure is illustrated in Fig. 2.

5 Results and discussion

In this section, the effect of various thermal and thermo-mechanical loading conditions on cyclic viscoplastic behavior of thick spherical vessels are investigated. The numerical responses of present work are verified with the experimental data for uniaxial loading condition and results of commercial finite element program.

5.1 Verification

Figure 3 shows the comparison between the results obtained in present work and the experimental data given in Hyde et al. (2014) for a service-aged P91 steel subjected to uniaxial strain cyclic loading under isothermal condition, 500 °C. The axial strain is cycled between -0.5% and 0.5% with $\dot{\epsilon}_x = 0.1\%/\text{s}$ strain rate and 120 s creep time after loading procedure. The Chaboche unified viscoplastic model is used and the material properties are assumed

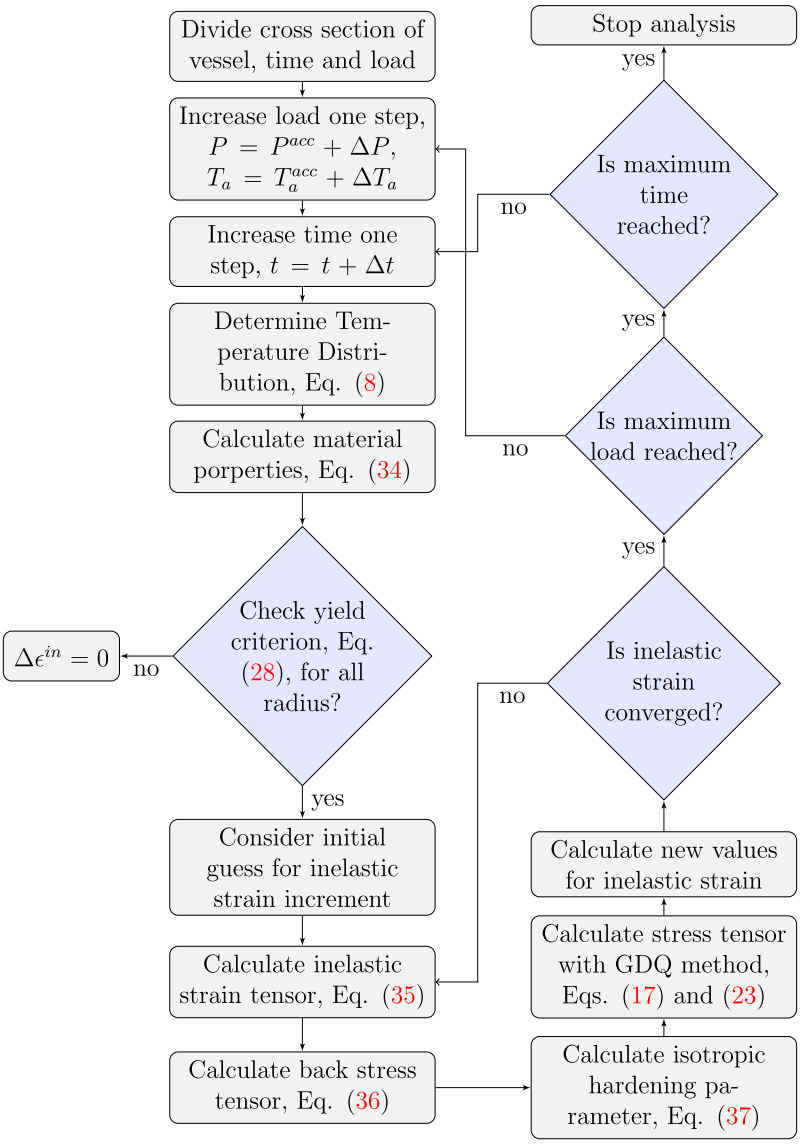

Fig. 2 Flow chart of the proposed numerical procedure

to be $\sigma_0 = 28.02$ MPa, $E = 156310$ MPa, $C_1 = 4607.47$, $C_2 = 379.69$, $a_1 = 45.04$ MPa, $a_2 = 109.72$ MPa, $n = 6.55$, $Z = 807.55$ MPa$\,s^{1/n}$, $b = 2.54$, $Q = -59.05$ MPa and $H = -1.84$. Figure 3 shows that the experimental data of Hyde et al. (2014) and numerical data of current work are in close agreement.

In order to demonstrate the accuracy of the proposed numerical method of the present work in evaluating inelastic responses of the structures, a commercial finite element program is used. In Figs. 4 and 5 a thick spherical vessel made of an alloy similar to U720Li alloy (Zhan and Tongi 2007) is subjected to thermal and thermo-mechanical loads, respec-

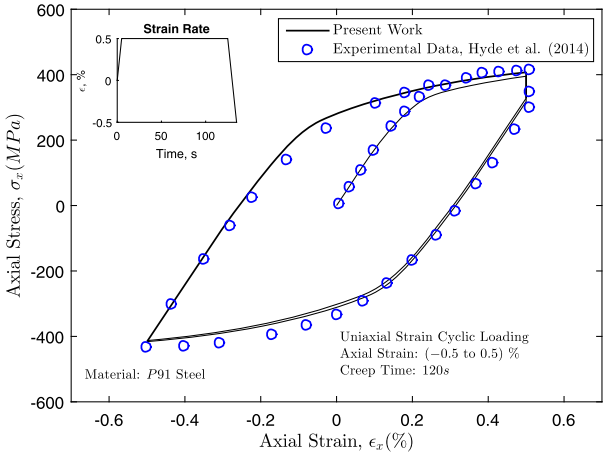

Fig. 3 Comparison of present work with the experimental data of beam given by Hyde et al. (2014)

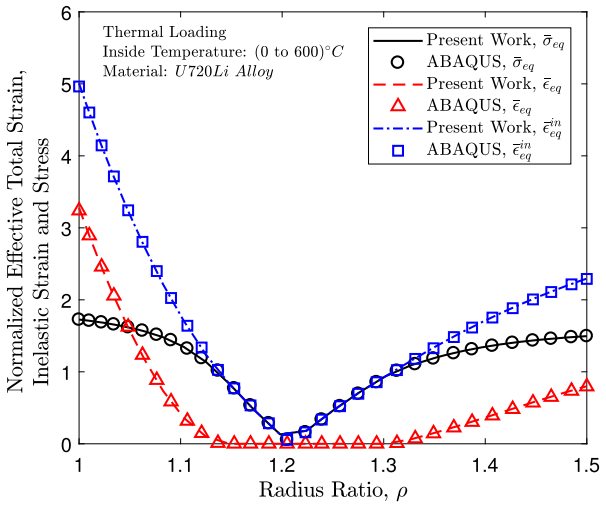

Fig. 4 Comparison of results of the thermal load of present work with ABAQUS

tively. The results of ABAQUS for the normalized effective total strain, inelastic strain, and stress versus radius ratio are depicted and compared with the results obtained through the present formulations. The material properties are: $\sigma_0 = 800$ MPa, $E = 509000$ MPa, $C_1.a_1 = 141590$, $C_2.a_2 = 688100$, $C_1 = 391.61$ MPa, $C_2 = 2578.69$ MPa, $b = 7.13$ and $Q = 161.52$ MPa. The back stresses due to this hardening model is defined by Eq. (44),

$$
\begin{aligned}
d\chi_{ij}^{(k)} &= C_k a_k(\sigma_{ij} - \chi_{ij})d\epsilon^p - C_k\chi_{ij}^{(k)}d\epsilon^p, \\
\chi_{ij} &= \sum_{k=1}^{m} \chi^{(k)}.
\end{aligned}
\tag{44}
$$

By substituting the aforementioned kinematic hardening given by Eqs. (44) in the numerical algorithm of present work and considering $\dot{\epsilon}^{in} = 0$, the plastic responses of present work are compared with the ABAQUS results. The maximum percentage of error between the FEM method and the proposed approach is less than 2%.

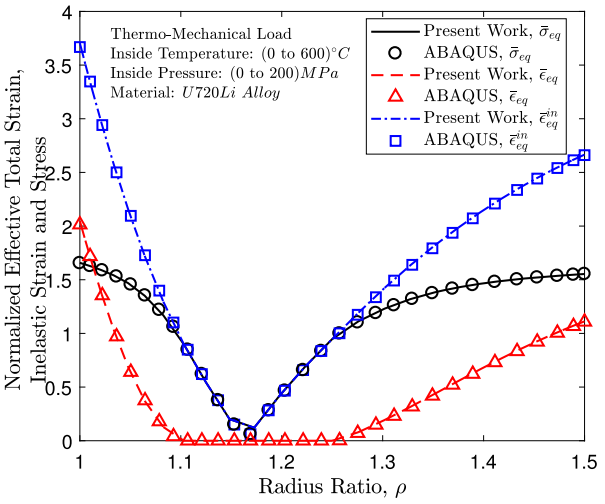

Fig. 5 Comparison of results of thermo-mechanical load of present work with ABAQUS

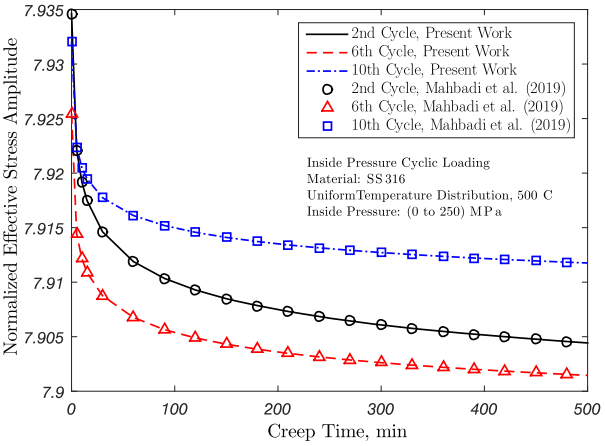

Fig. 6 Comparison viscoplastic results of present work with Mahbadi et al. (2018)

In Fig. 6 the viscoplastic response of present method is verified with Mahbadi et al. (2018), where a thick pressure vessel is subjected to mechanical cyclic loads. The inside pressure is cycled between 0 to 250 MPa under uniform temperature distribution. By comparison the method is well justified.

5.2 Viscoplastic cyclic behavior

In the following section, the cyclic viscoplastic behavior of thick spherical vessels made of 316 stainless steel subjected to thermo-mechanical loads is evaluated. The material properties of the unified Chaboche viscoplastic model are given in Table 1 (Gong et al. 2010). The radius ratio of the vessel is $\beta = 1.5$, H parameter in Eq. (32) is set to be zero and ξ_1 and ξ_2 in Eq. (7) are considered to be 0.0125 $\mathrm{W\,m^{-1}\,k^{-2}}$ and 15 $\mathrm{W\,m^{-1}\,k^{-1}}$, respectively.

Table 1 Material properties at multiple temperatures (Gong et al. 2010)

Temperatures (°C)	300 °C	500 °C	550 °C	600 °C
σ_0 (Mpa)	39	32.5	31	30
E (Gpa)	154.84	145.54	141.26	139.12
b	39.46	33.35	31	28.6
Q (Mpa)	32.76	30.41	27.8	27.43
a_1 (Mpa)	119.1	94.6	86.3	80.06
C_1	5964.1	6472.6	6939	7111.9
a_2 (Mpa)	108.4	113.3	114.8	116
C_2	1001.6	979.91	957.69	928.7
Z (Mpa s$^{\frac{1}{n}}$)	179	175	173	170
n	10	10	10	10

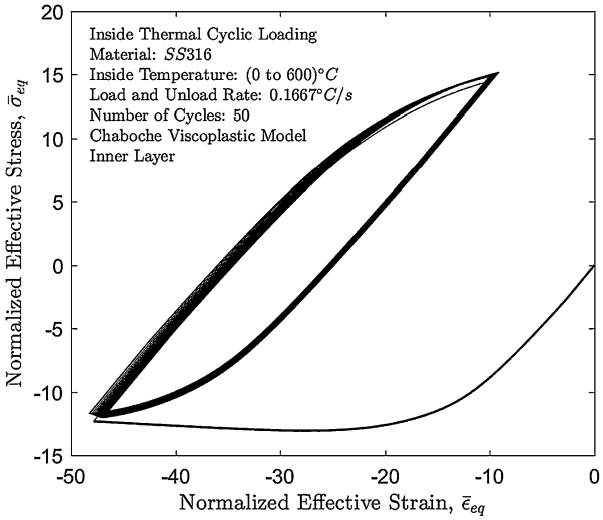

Fig. 7 Reverse plasticity due to the thermal cyclic loading without creep time in the inner layer

5.2.1 Pure thermal cyclic load without creep

The cyclic viscoplastic response of a spherical vessel subjected to the thermal cyclic loading, $T_i = 0$ to 600 °C, without considering creep time for the inner and outer layers are evaluated in Figs. 7 and 8. The loading and unloading rate is 0.1666 °C/s. The maximum effective strain and stress are occurred in the inner and outer layers, respectively. As shown in these figures, reverse plasticity is occurred in both critical points under this cyclic loading condition. In this situation, stress amplitude and strain amplitude remain the same by proceeding the cyclic loading further from the initial transient cycles. In these figures the ratcheting behavior is negligible after the first transient cycles, and the start of reversed plasticity may be considered after these transient cycles. The initial transient cycle for Figs. 7 and 8 is approximately the second and sixth cycles, respectively. In Figs. 7 and 8, the steady stress amplitude after the transient cycles is 13.61 (or 421.76 MPa) and 12.28 (or 380.5449 MPa), and the steady strain amplitude of reverse plasticity is 18.8955 (or 0.4165%) and 13.765 (or 0.3034%), respectively. Moreover, the start of reversed yielding in Figs. 7 and 8 is at 522.6 °C and 438.0 °C, respectively, and the magnitude of back stress

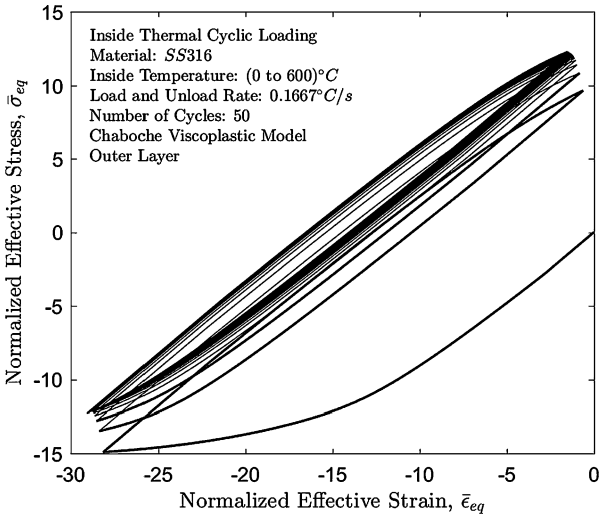

Fig. 8 Reverse plasticity due to the thermal cyclic loading without creep time in the outer layer

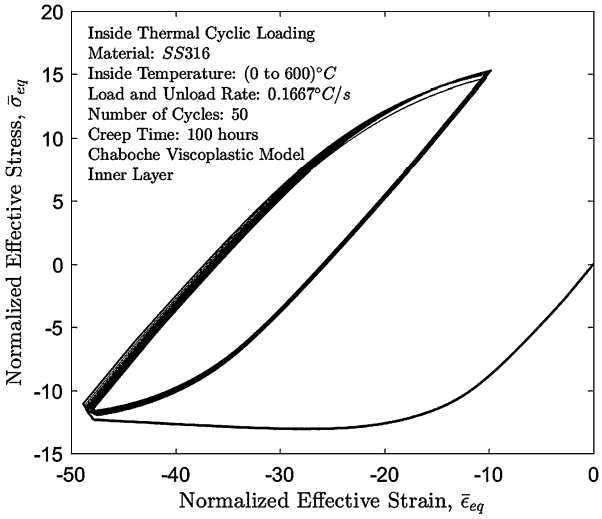

Fig. 9 Reverse plasticity due to the thermal cyclic loading with 100 h creep time in the inner layer

components and isotropic hardening parameter in these figures are $\chi = (\chi_{rr}, \chi_{\theta\theta}, \chi_{\phi\phi}) =$ (179.80, 89.90, 89.90) MPa, $R = 6.60$ MPa, and (23.76, 11.88, 11.88) MPa, $R = 1.41$ MPa, respectively, for the first cycle.

5.2.2 Pure thermal cyclic load with creep time

Figures 9 and 10 depict the normalized effective stress versus normalized effective strain of the inner and outer layers of the vessel. The vessel is under pure thermal cyclic loading with 100 hours creep time at the end of the loading condition. Similar to Figs. 7 and 8, reverse plasticity is observed in both layers and it is noted that creep time does not have major effect on the cyclic viscoplastic behavior of the vessel. The initial transient cycle for Figs. 9 and 10 is approximately the second and fifth cycles, respectively. In Figs. 9 and 10, the steady stress amplitude after the transient cycles is 13.66 (or 423.3097 MPa) and 12.315

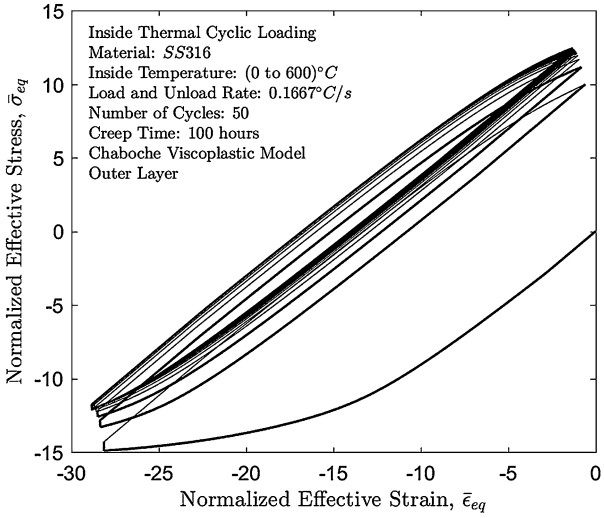

Fig. 10 Reverse plasticity due to the thermal cyclic loading with 100 h creep time in the outer layer

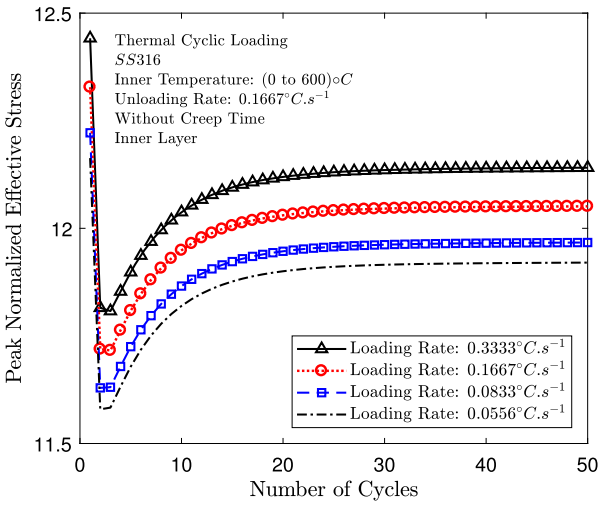

Fig. 11 Effect of loading rate on peak effective stress

(or 381.6295 MPa), and the steady strain amplitude of reverse plasticity is 19.0315 (or 0.4195%) and 13.774 (or 0.3036%), respectively. Moreover, the start of reversed yielding in Figs. 9 and 10 is at 535.6 °C and 456.2 °C and the magnitude of back stress components and isotropic hardening parameter in these figures are $\chi = (\chi_{rr}, \chi_{\theta\theta}, \chi_{\phi\phi}) = (186.90, 93.45, 94.45)$ MPa, $R = 6.86$ MPa and $(30.41, 15.21, 15.21)$ MPa, $R = 1.52$ MPa, respectively, for the first cycle.

5.2.3 Effects of loading rate

Peak normalize stress and strain versus number of cycles are illustrate in Figs. 11 and 12, respectively, for different loading rates but constant unloading rate. It is shown that increasing the rate of loading results into increase of the peak effective stress and decrease of the peak

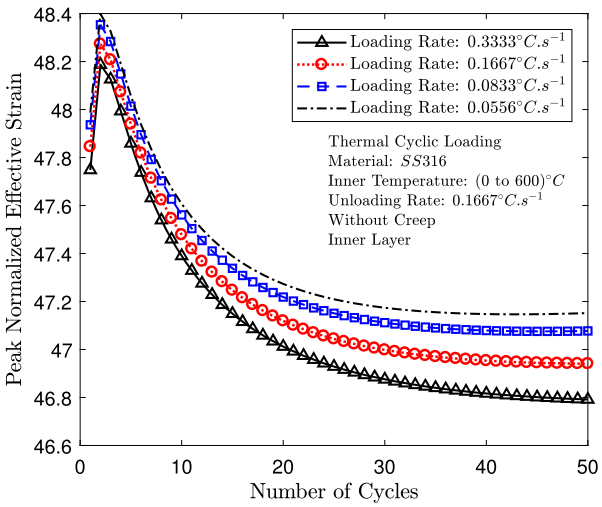

Fig. 12 Effect of loading rate on peak effective strain

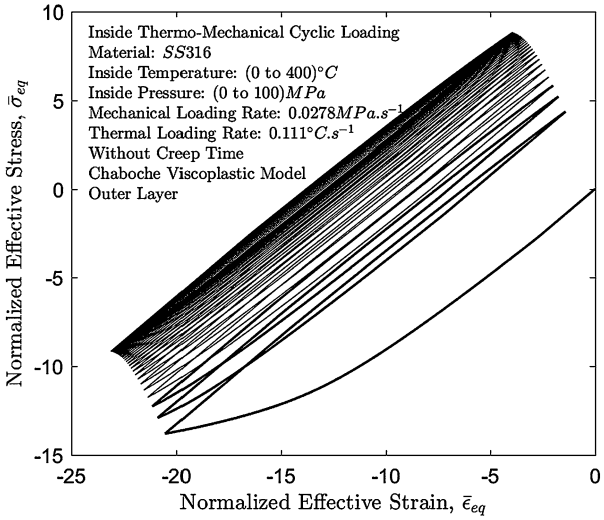

Fig. 13 Reverse plasticity due to the thermo-mechanical cyclic loading with domination of thermal load

effective strain. Also, it is concluded that the difference between loading and unloading rates have no major effect on the viscoplastic cyclic behavior and reverse plasticity is observed.

5.2.4 Thermo-mechanical cyclic loading

In order to evaluate the effects of mechanical and thermal loads on cyclic viscoplastic behavior of the vessel, the vessel is subjected to thermo-mechanical cyclic loading with higher thermal cyclic load. The inside temperature and pressure are cycled between 0 to 400 °C and 0 to 100 MPa, respectively. In this loading condition, the critical point takes place on the outer layer of the vessel. It is concluded that when thermal cyclic load is high enough compared to the mechanical cyclic load, the effective stress–strain cycle ratchets to a stabilized reverse plasticity cycle, as shown in Fig. 13 and 14. Figure 13 represents that the accumulated inelastic strain decreases in magnitude.

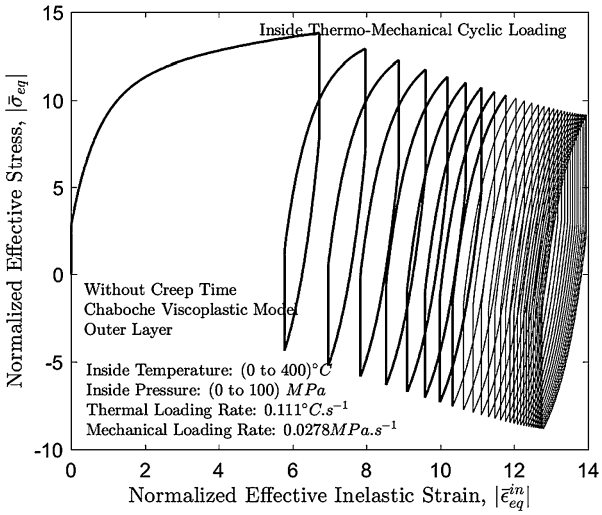

Fig. 14 Stabilizing of accumulated inelastic strain due to thermo-mechanical cyclic loading with domination of thermal load

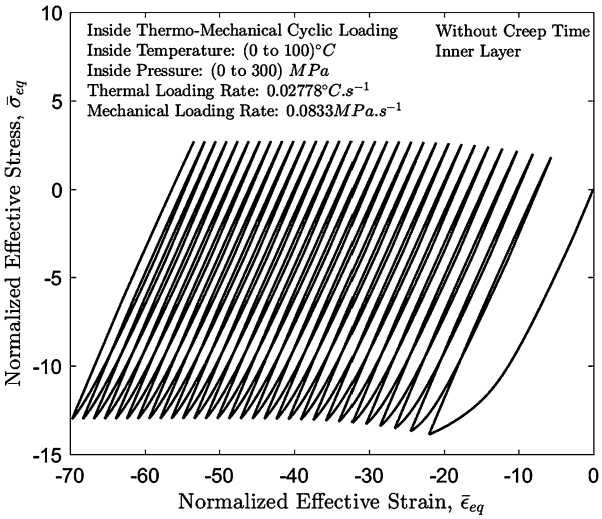

Fig. 15 Ratcheting behavior due to the thermo-mechanical cyclic loading with domination of the mechanical load

In Figs. 15 and 16, the spherical vessel is cycled under thermo-mechanical load, where the inside temperature is cycled between 0 and 100 °C and inside pressure is cycled between 0 and 300 MPa. Since the maximum effective stress and strain occur at the inner layer of vessel, this layer is the critical point in design problem. As a result of this loading condition, when the mechanical cyclic load dominates the thermal cyclic load, the effective strain is increased through each cycles, as shown in Fig. 15. Thus, ratcheting cyclic phenomenon is observed and inelastic strain is accumulated after each cycles. Figure 16 illustrates this accumulated inelastic strain.

5.2.5 Effect of material temperature dependency

The effects of the temperature dependence of material properties are investigated in this section. In Figs. 17 and 18, normalized peak effective stress and peak strain are shown in

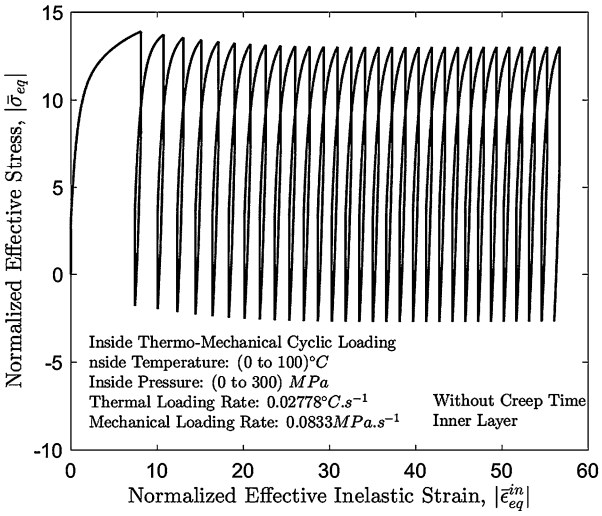

Fig. 16 Accumulation of inelastic strain due to thermo-mechanical cyclic loading with domination of the mechanical load

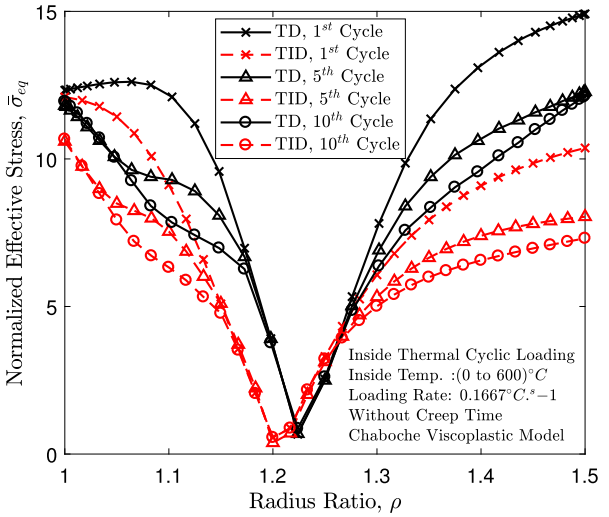

Fig. 17 Effect of considering temperature dependence on effective stress distribution along thickness

various radius and different cycles when material temperature dependence is considered and when it is not considered. If the material properties are considered to be independent of the temperature, there would be an extreme difference between these responses and the results of temperature-dependent material. The maximum differences between the results of these two material properties are about 30% for effective stress and 40% for effective strain. While there are significant differences between the magnitudes of stresses and strains, the reverse plasticity behavior is observed for both conditions due to the thermal cyclic loading.

6 Conclusion

Applying the compatibility and equilibrium equations, the governing differential equations are solved using the GDQ method in order to obtain strain and stress distributions along

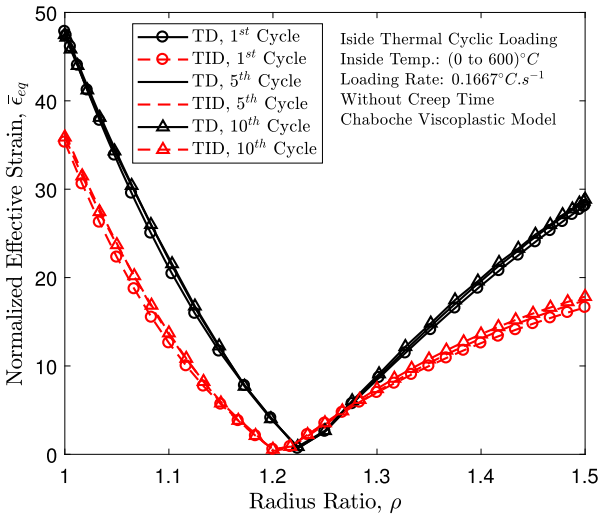

Fig. 18 Effect of considering temperature dependence on effective strain distribution along thickness

the thickness of the spherical vessels subjected to thermos-mechanical loads. The unified Chaboche viscoplastic model with combined isotropic and kinematic hardening theories is used to evaluate the inelastic strains. A numerical iterative method with consideration of the GDQ method to solve differential equations is proposed which is quite capable and efficient to handle the cyclic loading analysis of the viscoplastic structures. In regard to the field of cyclic inelastic behavior of the structures, cyclic viscoplastic responses of a thick spherical vessel due to thermal and thermo-mechanical loading conditions considering creep time are investigated employing the proposed numerical method. The outputs of present numerical procedure are verified by some experimental data and a commercial finite elements program. The novelty of the present study, in comparison with the published papers reported on thermal cyclic loading, is the application of a rate-dependent constitutive model considering temperature dependence of material properties and employing the GDQ method to calculate the stress and strain tensors. The results of cyclic viscoplastic behavior analysis for the spherical thick vessels are summarized in the following:

- Similar to the plasticity cyclic behavior, cyclic viscoplasticity predicts reverse plasticity for vessels under thermal cyclic load, where the stress classification is of strain controlled type.
- While the unified Chaboche viscoplastic model predicts shakedown for thermal cyclic loading, ratcheting behavior could be observed under thermo-mechanical cyclic loading when mechanical load (load-controlled) dominates the thermal load.
- Creep time and difference between loading and unloading rates do not have significant impact on the cyclic viscoplastic behavior (i.e. ratcheting, reverse plasticity). However, they have influence on the strain and stress distributions.
- Temperature dependence of material properties plays an important role to evaluate the stresses and strains of the vessel and to recognize the critical points.

References

Ahmed, R., Barrett, P.R., Hassan, T.: Unified viscoplasticity modeling for isothermal low-cycle fatigue and fatigue-creep stress–strain responses of Haynes 230. Int. J. Solids Struct. **88–89**, 131–145 (2016)

Armstrong, P.J., Frederick, C.O.: A mathematical representation of the multiaxial Bauschinger effect. Technical Report CEGB Report No. RD/B/N 731 (1966)

Bellman, R., Casti, J.: Differential quadrature and long-term integration. J. Math. Anal. Appl. **34**, 235–238 (1971)

Benaarbia, A., Rouse, J.P., Sun, W.: A thermodynamically-based viscoelastic-viscoplastic model for the high temperature cyclic behaviour of 9–12% Cr steels. Int. J. Plast. **107**, 100–121 (2018)

Besseling, J.F.: A theory of elastic, plastic and creep deformations of an initially isotropic material showing anisotropic strain hardening, creep recovery and secondary creep. Trans. ASME J. Appl. Mech. **25**, 529–563 (1959)

Chaboche, J.L.: Time-independent constitutive theories for cyclic plasticity. Int. J. Plast. **2**, 149–188 (1986)

Chaboche, J.L., Rousselier, G.: On the plastic and viscoplastic constitutive equation part 1: rules developed with internal variable concept. J. Press. Vessel Technol. **105**, 153–158 (1983a)

Chaboche, J.L., Rousselier, G.: On the plastic and viscoplastic constitutive equation part 2: application of internal variable concept to the 316 stainless steel. J. Press. Vessel Technol. **105**, 159–164 (1983b)

Chen, W., Feng, M.: A study of a cyclic viscoplasticity model based on hyperbolic sine form for the inelastic strain rate. Int. J. Mech. Sci. **101–102**, 155–160 (2015)

Chen, W., Wang, F., Kitamura, T., Feng, M.: A modified unified viscoplasticity model considering time-dependent kinematic hardening for stress relaxation with effect of loading history. Int. J. Mech. Sci. **133**, 883–892 (2017)

Chen, W., Kitamura, T., Feng, M.: Creep and fatigue behavior of 316L stainless steel at room temperature: experiments and a revisit of a unified viscoplasticity model. Int. J. Fatigue **112**, 70–77 (2018)

Cruzado, A., Llorca, J., Segurado, J.: Modeling cyclic deformation of inconel 718 superalloy by means of crystal plasticity and computational homogenization. Int. J. Solids Struct. **122**, 148–161 (2017)

Dang-Ban, K., Chaboche, J.L., Coridier, G.: Modelization of the strain memory effect on the cyclic hardening of 316 stainless steel. In: Proceedings of the 5th International Conference on SMiRT, Germany (1979)

Dong, C., Yang, X., Shi, D., Yu, H.: Modeling of anisotropic tensile and cyclic viscoplastic behavior of a nickel-base directionally solidified superalloy. Mater. Des. **55**, 966–978 (2014)

Gong, Y.P., Hyde, C.J., Sun, W., Hyde, T.H.: Determination of material properties in the Chaboche unified viscoplasticity model. J. Mater. Des. Appl. **224**, 19–29 (2010)

Hang, L.D., Guang, S.D., Gao, L.Z., Jie, W.J., Jie, H., Dong, L.X., Qiang, T.Z., Cheng, Z.C., Bo, C.: Unified viscoplastic constitutive model under axial-torsional thermo-mechanical cyclic loading. Int. J. Mech. Sci. **90**, 102–150 (2019)

Hashiguchi, K.: Foundations of Elastoplasticity: Subloading Surface Model. Springer, Berlin (2017)

Hetnarski, R.B., Eslami, M.R.: Thermal Stresses—Advanced Theory and Applications. Springer, Berlin (2019)

Hill, R.: The Mathematical Theory of Plasticity. Oxford University Press, London (1950)

Hyde, C.J., Sun, W., Hyde, T.H., Rouse, J.P., Farragher, T., O'Dowd, N.P., Leani, S.B.: Cyclic viscoplasticity testing and modeling of a service-aged P91 steel. J. Press. Vessel Technol. **136**(4), 044501 (2014)

Karlsson, B.I., Hibbit, H.D., Sorensen, P.: Abaqus User's Manual. HKS Inc., Dallas (2001)

Kashef, B., Bellman, R., Casti, J.: Differential quadrature: a technique for the rapid solution of nonlinear partial differential equations. J. Comput. Phys. **10**, 40–52 (1972)

Kyaw, S.T., Rouse, J.P., Lu, J., Sun, W.: Determination of material parameters for a unified viscoplasticity-damage model for a P91 power plant steel. Int. J. Mech. Sci. **115–116**, 168–179 (2016)

Lemaitre, J.: Handbook of Materials Behavior Models. Academic Press, San Diego (2001)

Luk-Cyr, J., Paquet, D., Lanteigne, J., Champliaud, H., Vadean, A.: A unified plasticity methodology for rate- and temperature-sensitive alloys exhibiting a non-linear kinematic hardening behavior. Acta Mech. Solida Sin. **30**, 27–37 (2017)

Mahbadi, H., Eslami, M.R.: Cyclic loading of thick vessels based on the Prager and Armstrong–Frederick kinematic hardening models. Int. J. Press. Vessels Piping **83**, 409–419 (2006)

Mahbadi, H., Komijani, M., Eslami, M.R.: Thermal and mechanical cyclic loading of thick spherical vessels made of transversely isotropic materials. Int. J. Press. Vessels Piping **107**, 1–11 (2013)

Mahbadi, H., Ejtemajou, M., Eslami, M.R.: Load controlled cyclic loading of transversely isotropic cylindrical vessels based on the anisotropic kinematic hardening models. J. Press. Vessel Technol. **139**, 031402 (2017)

Mahbadi, H., Falahi, V., Eslami, M.R.: Ratcheting responses of spherical vessels under load controlled condition based on the Chaboche viscoplastic model. Trans. of ISME (2019). Submitted

Mroz, Z.: On the description of anisotropic work hardening. J. Mech. Phys. Solids **15**, 163–175 (1967)

Neal, K.W., Shirvastava, S.C.: Analytical solutions for circular bars subjected to large strain plastic torsion. ASME J. Appl. Mech. **57**, 298–306 (1990)
Parger, W.: A new method of analyzing stresses and strains work-hardening plastic solids. J. Appl. Mech. **23**, 493–496 (1958)
Rae, Y., Benaarbia, A., Hughes, J., Sun, W.: Experimental characterisation and computational modelling of cyclic viscoplastic behaviour of turbine steel. Int. J. Fatigue **124**, 581–594 (2019)
Roostaei, A.A., Jahed, H.: A cyclic small-strain plasticity model for wrought Mg alloys under multiaxial loading: numerical implementation and validation. Int. J. Mech. Sci. **145**, 318–329 (2018)
Rusinko, A., Rusinko, K.: Synthetic theory of irreversible deformation in the context of fundamental bases of plasticity. Mech. Mater. **41**, 106–120 (2009)
Rusinko, A., Rusinko, K.: Plasticity and Creep of Metal. Springer, Berlin (2011)
Shojaei, A., Eslami, M.R., Mahbadi, H.: Cyclic loading of beams based on the Chaboche model. Int. J. Mech. Mater. Des. **6**, 217–228 (2010)
Shorr, B.F.: Thermal Integrity in Mechanics and Engineering. Foundations of Engineering Mechanics. Springer, Berlin (2015)
Shu, C.: Differential Quadrature and Its Application in Engineering. Springer, Berlin (2012)
Szmytka, F., Forre, A., Augustins, L.: A time increment control for return mapping algorithm applied to cyclic viscoplastic constitutive models. Finite Elem. Anal. Des. **102**(103), 19–28 (2015)
Westergaard, H.M.: Theory of Elasticity and Plasticity. Harvard University Press, Cambridge (1952)
Xiaoan, H., Qiang, Z., Xiao-Guan, Y., Duo-Qi, S.: Viscoplastic analysis method of an aero-engine turbine blade subjected to transient thermo-mechanical loading. Int. J. Mech. Sci. **152**, 247–256 (2019)
Zhan, Z.: A study of creep–fatigue interaction in a new nickel-based superalloy. PhD thesis, University of Portsmouth (2004)
Zhan, Z.L., Tongi, J.: A study of cyclic plasticity and viscoplastic in a new nickel based superalloy using unified constitutive equations. Part I: evaluation and determination of material parameters. Mech. Mater. **39**, 64–72 (2007)
Zhan, L., Tong, Z., Vermeulen, B.: Modelling of cyclic plasticity a viscoplasticity of a nickel-based alloy using Chaboche constitutive equations. Int. J. Fatigue **26**, 829–837 (2004)
Zheng, X., Wang, W., Guo, S., Xuan, F.: Viscoplastic constitutive modelling of the ratcheting behavior of 35CrMo steel under cyclic uniaxial tensile loading with a wide range of stress amplitude. Eur. J. Mech. A, Solids **76**, 312–320 (2019)
Zhu, Y., Kang, G., Kan, Q., Bruhns, O.T., Liu, Y.: Thermo-mechanically coupled cyclic elasto-viscoplastic constitutive model of metals: theory and application. Int. J. Plast. **79**, 111–152 (2016)
Ziegler, H.: A modification of Prager's hardening rule. Q. Appl. Math. **17**, 55–60 (1959)